RSC Advances

ROYAL SOCIETY OF CHEMISTRY

www.rsc.org/advances

Graphic Abstract

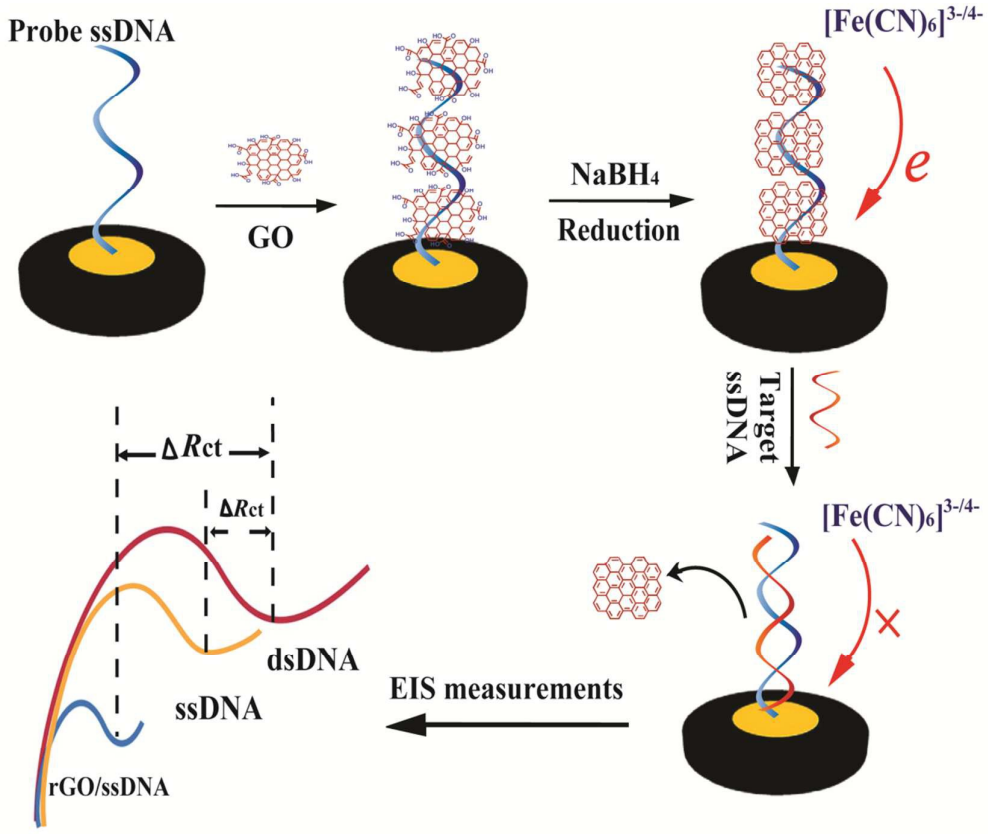

A facile and highly sensitive impedimetric DNA bosensor with ultralow background response based on in-suit reduced graphene oxide

Journal Name

ARTICLE

A facile and highly sensitive impedimetric DNA biosensor with ultralow background response based on *in-situ* reduced graphene oxide

Received 00th January 20xx,
Accepted 00th January 20xx

DOI: 10.1039/x0xx00000x

www.rsc.org/

Aiqun Wu, Qingxiang Wang*, Qionghua Zhu, Jiancong Ni, Feng Gao

A novel electrochemical impedimetric DNA sensor was constructed based on *in-situ* chemical reduction of graphene oxide (GO) that had been attached at DNA modified electrode. First, the mercapto-modified probe DNA was anchored on a gold electrode surface through the Au-S bond. Then the GO was adsorbed on the probe DNA through the unique π-π stacking, which was followed by incubation in sodium borohydride ($NaBH_4$) solution to *in-suit* reduce the GO to the reduced form (rGO). Thus, a highly conductive biointerface with ultralow charge-transfer resistance was obtained. When the biosensor was hybridized with the target DNA to form the rigid double-strand DNA, the rGO was released from the electrode surface and the charge-transfer resistance increased again. Compared with the analogous sensing interface without pre-accumulation of GO, the signal variation ratio was found to increase by 8-fold upon hybridization as determined by electrochemical impedance spectra, suggesting a higher signal-to-noise of the constructed biosensor. Quantitative analysis experiments showed that the impedance change values exhibited a good linear relationship with the logarithmic values of target DNA concentration over the wide range from 1.0×10^{-15} M to 1.0×10^{-9} M. The detection limit was estimated to be as low as 2.9×10^{-16} M. The biosensor also presented excellent selectivity, good regeneration ability and outstanding stability.

1 Introduction

In recent decade, the accurate and rapid detection of specific DNA has attracted intensive interest in the field of biomolecular sensing owing to its important role in genetic-disease diagnosis, drug screening, food and environment monitoring. Electrochemical DNA biosensors offer a great promise for DNA analysis because of its simplicity, rapidness, low-cost and easiness to miniaturize. To date, a lot of efforts have been directed toward the development of high-powered electrochemical DNA sensors.[1-3] Apart from the label-free methods,[4-6] the strategies making use of labels like ferrocene,[7] enzymes,[8] nanoparticles,[9] and metal complexe[10] to amplify the electrochemical responses of the sensors have been intensively investigated. However, although the labeling strategy greatly improves the sensor sensitivity, it also markedly increased the operation time, complexity, and cost of the experiments. In contrast, the label-free biosensors are more appropriate for the practical application as an analytic tool.

Electrochemical impedance spectroscopy (EIS) transduction technique has been regarded as a powerful technique for the characterization of electrochemical systems and functionalization of bio-electrodes.[11-13] Due to its merits of portability, low-cost, and simplicity, it has also been successfully applied for the analysis of enzymes,[14,15] tumor markers,[16,17] and heavy metals.[18,19] Since the unique DNA hybridization reaction can cause the changes of the charges, conductivity and microenviroment situation of the biointerface, the EIS has also received considerable attention in DNA analysis. However, the traditional hybridization-based EIS biosensors suffer from a few shortages and limitations. For example, the non-specific adsorption of some interferents on the electrode surface will also change the situation of the biointerface, resulting in the variation of EIS

Department of Chemistry and Environment Science, Fujian Province University Key Laboratory of Analytical Science Minnan Normal University, Zhangzhou, 363000 P. R. China
Email:axiang236@126.com

response and the false-positive results. On the other hand, the high negative-charge density of the probe electrode can cause a large background in EIS measurement, which makes the detection less sensitive. Therefore, it is still a great challenge to develop novel strategy to improve the analytic performance of the impedimetric DNA biosensor.

Graphene oxide (GO), a layered carbon-based compound, has attracted intensive attention in biological applications in recent years, owing to its outstanding characteristics such as good water dispersibility, outstanding fluorescent property, high mechanical strength, and facile surface modification.[20-22] It has been reported that GO could bind with single-stranded DNA (ssDNA) via hydrophobic and π-stacking interactions. Base on this, some new sensing systems have been exploited for the detection of proteins,[23] DNA,[24,25] small molecules[26] or ions[27] using ssDNA as the recognition element. For example, Alessandra and co-workers[24] have demonstrated an electrochemical biosensing platform for single nucleotide polymorphism detection based on the inherently electroactivity of GO. Based on the proposed platform, they utilized the reduction signal of GO for the detection of DNA hybridization and polymorphism. Recently, Luo and co-workers[25] presented a label-free electrochemical aptasensor based on methylene blue-anchored GO amplification for thrombin (TB) and adenosine triphosphate (ATP) detection, which took the advantages of the specific affinity of the aptamer towards the target and the different affinities of GO with ssDNA and dsDNA/G-quadruplex. However, these early sensors still possessed some disadvantages, such as high over-potential and inferior electrochemical signals of GO, low electrical conductivity and large background response.

To overcome these problems, Dong and co-workers[28] constructed a new electrochemical biosensing platform based on the unique interaction of ssDNA with the highly conductive graphene (GR). The results showed that the adsorption of GR on the adenosine triphosphate binding aptamer (ABA) immobilized electrode caused a large decrease of the charge transfer resistance (R_{ct}) in impedance test, resulting in very low background response and high sensitivity for ATP determination. Nevertheless, the direct use of GR as the sensing platform also has some disadvantages. First, on the most common and economical chemical reduction method to prepare GR, the hazardous chemical of hydrazine[29,30] is needed as a reductant, which not only increases the operating procedures of assays, but also possesses the potential risk of environmental pollutant. More important, GR is hydrophobic and tends to form irreversible agglomerates or even restack to form graphite through strong π-π stacking or van der Walls interaction under certain conditions, which decreased the stability and reproducibility of the biosensor.[31]

Herein, we construct a facile impedimetric DNA biosensor with ultralow background response on the basis of *in-situ* reduction of graphene oxide to the reduced form (rGO) at the sensing interface (Scheme 1). First, the mercapto-modified probe DNA was anchored on a gold electrode surface through to the Au-S bond. Then the GO with excellent homogeneity and water-solubility was adsorbed on the probe DNA through the unique π-π stacking, which was followed by *in-situ* incubation of sodium borohydride ($NaBH_4$) solution to reduce the GO to rGO. Thus, a highly conductive biointerface with ultralow charge-transfer resistance in impedance test was obtained. Compared with sensor without rGO, the signal variation ratio was increased by 8-fold in hybridization reaction, suggesting a higher signal-to-noise of the designed sensor. Quantitative analysis experiments showed that the impedance change values have good linear relationship with the logarithmic values of target DNA concentration in the range from 1.0×10^{-15} M to 1.0×10^{-9} M. The detection limit was estimated to be as low as 2.9×10^{-16} M. The selectivity experiment showed the biosensor also exhibited good recognition for complementary, one-base, three-base mismatched and non-complementary DNA. This concept can also be extended to be employed for the construction of other oligonucleotides-based biosensors (such as aptasensors) for the detection of proteins, metal ions, cells and RNAs.

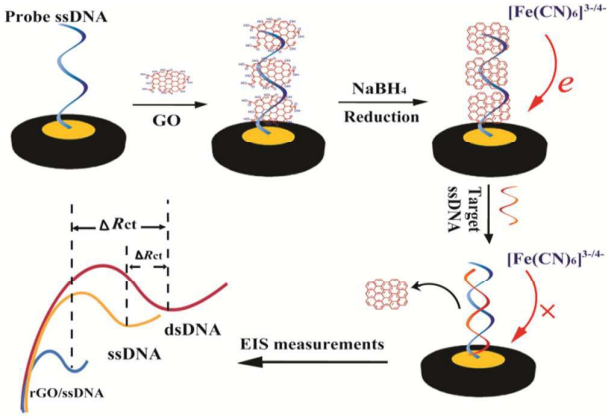

Scheme 1 Illustration for the fabrication and hybridization detection of the DNA biosensor based on in-situ reduction of graphene oxide.

2 Experimental

2.1 Reagents and apparatus

Graphite, ethylenediaminetetraacetic acid (EDTA), $K_4[Fe(CN)_6]$ and $K_3[Fe(CN)_6]$ were obtained from Xilong Chemical Co., Ltd (China). 6-mercapto-1-hexanol (MCH) and Tris(2-carboxyethyl)phosphine hydrochloride (TCEP) were purchased from Sigma-Aldrich (China). Sodium borohydride ($NaBH_4$) was provided by Shanghai Chemical Reagent Co., Ltd (China). The graphene oxide (GO) was prepared according to a modified Hummer's method using graphite power as the original material.[32] Doubly distilled water (DDW) was used throughout the experiment.

The 18-base synthetic oligonucleotides related to CaMV35S promoter gene were provided by Shanghai Sangon Bio-engineering Co., Ltd (China).

- Mercapto-modified probe DNA (S1): 5'-SH-$(CH_2)_6$ - TCT TTG GGA CCA CTG TCG-3'
- Complementary sequence (S2): 5'-CGA CAG TGG TCC CAA AGA-3'
- One-base-mismatch sequence (S3): 5'-CGA CAG TGG TCC CAA CGA-3'
- Three-base-mismatch sequence (S4): 5'-CGA CAA TGG CCC CAA CGA-3'
- Non-Complementary sequence (S5): 5'-GCA TCC AGC GAG CAC GTA-3'

Stock solution (10 μM) of probe DNA was prepared with IB buffer solution (25 mM Tris-HCl, 100 mM NaCl, 100 mM $MgCl_2$, 10 mM TCEP, pH = 8.0) and kept frozen. The stock solutions of the other DNA oligonucleotides were prepared with TE buffer solution (0.01 M Tris-HCl, 0.01 M EDTA, pH 8.0) and also kept frozen, which was diluted with TE buffer solution before use.

Raman spectra were recorded on a Renishaw invia Raman microscope (UK). Electrochemical measurements were performed on a CHI 650C electrochemical workstation (China) at room temperature with a three-electrode system consisted of a bare or modified gold electrode (AuE, Φ=3.0 mm in diameter) as working electrode, a platinum wire as auxiliary electrode and Ag/AgCl as reference electrode.

2.2 Construction of the DNA biosensor

Before modification, the bare AuE was polished to a mirror-like surface with 1.0 μm, 0.3 μm and 0.05 μm alumina sequentially, and then ultrasonicated in DDW, ethanol and DDW in turn for 5min. After dried under N_2 flow, the freshly polished electrode was dipped in Piranha solution (98%H_2SO_4/30%H_2O_2, 7:3 (*V/V*)) for 20 min, and subsequently electrochemically cleaned between -0.2 to +1.5 V in 0.5 M H_2SO_4 until stable cyclic voltammetric (CV) curves were obtained. After being rinsed with DDW and dried with N_2 flow, the cleaned electrode was immediately immersed into 0.1 μM S1 solution for 24 h at 4 ℃ to assemble the probe DNA through the Au-S bond. After that, the electrode was rinsed with DDW to remove the physically adsorbed DNA. The obtained electrode was denoted as S1/AuE. Then the S1/AuE was immersed in 1 mM MCH for 2 h to block the electrode surface uncovered by S1, which was denoted as MCH-S1/AuE.

For assembly of GO, the prepared MCH-S1/AuE was immersed into 0.1 mg mL^{-1} GO for 3 h. After gentle rinsing with DDW to remove the loosely attached GO, the GO assembled electrode (GO/MCH-S1/AuE) was prepared. Followed by, the GO/MCH-S1/AuE was immersed into 0.1 M $NaBH_4$ solution for 35 min to *in-situ* transform the GO to the reduced form (rGO). After further rinsing with TE buffer solution, the probe electrode with assemblied rGO (rGO/MCH-S1/AuE) was obtained.

2.3 Hybridization and electrochemical measurements

The hybridization processes of the biosensor were performed by immersing rGO/MCH-S1/AuE into 100 μL analyte solution (S2, S3, S4 or S5) with desired concentrations for 45 min at 30 ℃, and then rinsed with TE buffer to remove the unhybridized DNA.

The stepwise fabrication of the biosensor was characterized by CV and EIS. The CV was scanned between -0.2 and 0.6 V with the scan rate of 1.0 V s^{-1}. The EIS was collected at a potential of +0.169 V in the frequency range from 0.01 to 10^5 Hz with the voltage amplitude of 5 mV. The supporting electrolyte was 1 mM $[Fe(CN)_6]^{3-/4-}$ (1:1) with 0.1 M KCl. The hybridization performance of the developed biosensor was monitored with EIS with the same conditions.

3 Results and discussion

3.1 Electrochemical characterization on the fabrication of the biosensor

The fabrication process of the biosensor was electrochemically characterized using $[Fe(CN)_6]^{3-/4-}$ as the redox probe. The CV and EIS results are showed in Fig. 1A and Fig. 1B, respectively. For the bare AuE, a couple of well-defined redox peaks of $[Fe(CN)_6]^{3-/4-}$

with the peak-to-peak separation (ΔE_p) of 75 mV were observed (Fig. 1A, curve a). When the bare AuE was treated with the probe DNA (S1), the redox peaks of $[Fe(CN)_6]^{3-/4-}$ showed obvious decrease (Fig. 1A, curve b), indicating that the probe DNA of S1 had been successfully immobilized on the AuE surface via the Au-S chemistry, and the negatively charged phosphate backbones of S1 blocked the approaching of $[Fe(CN)_6]^{3-/4-}$ ions to the electrode surface. While on MCH-S1/AuE, the redox peak intensity of $[Fe(CN)_6]^{3-/4-}$ further decreased and the peak-to-peak separation was also enlarged (Fig. 1A, curve c), indicating that MCH has been modified on the electrode surface to fill the unoccupied gaps on the AuE surface. After the GO was adsorbed on the probe DNA through the unique π-π stacking, it was found that the redox peak currents decreased again (Fig. 1A, curve d). This could be explained by the fact that the electrochemistry of the electroactive $[Fe(CN)_6]^{3-/4-}$ ions was inhibited by the poor conductivity of GO and the electrostatic repulsion from the negative -COOH group of GO. However, after GO/MCH-S1/AuE was incubated in $NaBH_4$ solution, the redox peaks of $[Fe(CN)_6]^{3-/4-}$ increased obvisouly, and the ΔE_p decreased (Fig. 1A, curve e). This suggested that the attached GO had been successfully reduced to rGO and enhanced the electron transfer kinetic of the electroactive probes on the electrode surface.

EIS can provide sensitive information about the change of the interface property. A typical Nyquist diagram is consisted of an oblique line at the low frequencies region that corresponds to the diffusion process, and a semicircle portion at high frequencies region that corresponds to the electron transfer limiting process. The charge transfer resistance (R_{ct}) value is often directly determined by measuring the diameter of the semicircle portion.[33] Figure 1B depicted the typical Nyquit plots of the AuE upon stepwise assembly of different materials. As seen, almost a straight line was observed for bare AuE (Fig. 1B, curve a), suggesting that the electroactive probe of $[Fe(CN)_6]^{3-/4-}$ underwent an absolute diffusion-limited electrochemical process on this electrode. While at S1/AuE, a large semicircle corresponding to the R_{ct} value of 49.9 kΩ was found (Fig. 1B, curve b), indicating that the coated layer of S1 on the electrode surface blocked the approaching of $[Fe(CN)_6]^{3-/4-}$ to electrode surface due to the electrostatic repulsion force. When MCH molecules were further assembled onto the interface, the R_{ct} value increased to 58.5 kΩ (Fig. 1B, curve c), which could be explained by the successful covering of residue sites of AuE surface by the MCH. In a DNA biosensor, this can effectively improve the analytical performance of the biosensor through avoiding the nonspecific adsorption of interferents, and erecting the probe DNA to have a better orientation for hybridization reaction. After the modified electrode was incubated in GO solution for 3 h, it was found that the R_{ct} showed a further increase with the value of 112.8 kΩ (Fig. 1B, curve d). This suggested that the GO had also been successfully attached on MCH-S1/AuE though the π-π stacking with S1, and inhibited the electron transfer of the $[Fe(CN)_6]^{3-/4-}$ on the electrode surface.

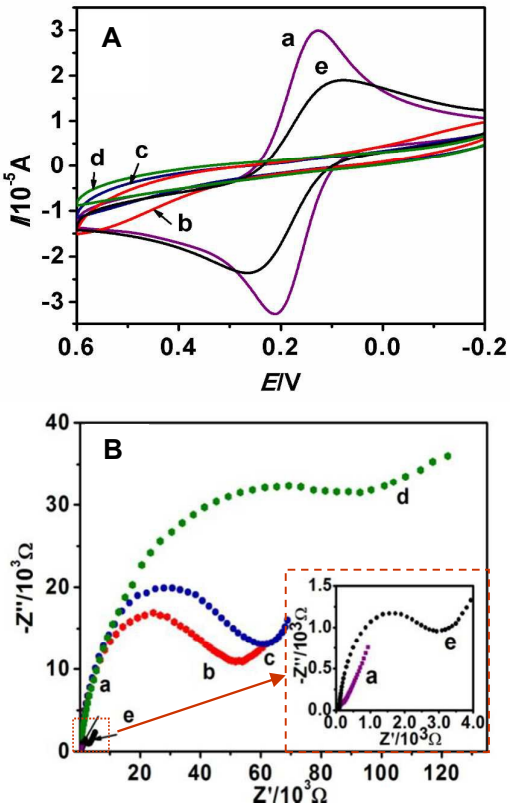

Fig. 1 Cyclic voltammograms (A) and Nyquist diagrams (B) of bare AuE (a), S1/AuE (b), MCH-S1/AuE (c), and GO/MCH-S1/AuE (d), rGO/MCH-S1/AuE (e) in 1.0 mM [Fe(CN)6]3-/4- solution containing 0.1 M KCl.

As a control, the AuE modified with only MCH layer (MCH/AuE) was also fabricated and incubated in GO solution. But under the same conditions, only a small increase of R_{ct} was observed (data not shown). This testified that GO were adsorbed onto the electrode surface mainly through the interaction with the probe DNA. In addition, after the GO modified electrode was incubated in $NaBH_4$ solution for 30 min, a substantial decrease of R_{ct} with the value of 3.5 kΩ was observed (Fig. 1B, curve e), which suggested

that the electron transfer of $[Fe(CN)_6]^{3-/4-}$ on the electrode surface had been significantly enhanced. And it could be ascribed to the successful formation of highly conductive rGO on the electrode surface through *in-situ* reduction of GO by $NaBH_4$. On the other hand, the ultralow R_{ct} value on rGO/MCH-S1/AuE also meant that the fabricated DNA biosensor had a small background response in EIS-based hybridization measurements, which would be very favorable to improve the sensitivity of the biosensor.

3.2 Hybridization feasibility and the improved signal variation ratio (SVR) of the biosensor

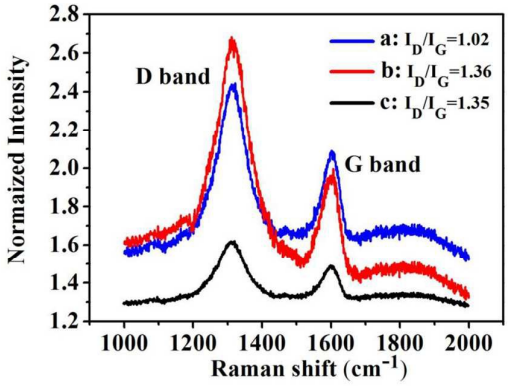

Fig. 2 Raman spectra of GO/MCH-S1/AuE (a), and rGO/MCH-S1/AuE before (b) and after hybridization with target DNA (c).

It has been reported that GO or rGO has specific interaction with ssDNA rather than dsDNA.[24,25] Therefore we supposed that after hybridization of the probe ssDNA with the target DNA on the electrode surface, the attached rGO would fall off from the electrode surface. In order to testify this speculation, the changes of the electrode surface upon reduction and hybridization were characterized by Raman spectra. Figure 2 shows the Raman spectra of GO/MCH-S1/AuE (a) and rGO/MCH-S1/AuE before (b) and after hybridization with target DNA (c). From the figure, it was clearly seen that two characteristic peaks, i.e., the G band at 1585 cm^{-1} assigning to the E_{2g} phonon of C sp^2 atoms and the D band at 1320 cm^{-1} corresponding to the breathing mode of κ-point phonons of A_{1g} symmetry were appeared at GO/MCH-S1/AuE, confirming that the GO has been successfully attached on the electrode surface. The intensity ratio of the D to G band (I_D/I_G) is determined to be 1.02. However, at the $NaBH_4$ reduced electrode (rGO/MCH-S1/AuE), it was found that the value of I_D/I_G was increased to 1.36, suggesting that the graphitization degree of the carbonaceous material on the electrode surface become higher.[34] This also meant that the GO has been changed to the reduced form after treatment by the strong reduction reagent of $NaBH_4$. When the electrode of rGO/MCH-S1/AuE was incubated in target DNA solution, the D band and G band were still visible and the value of I_D/I_G was almost the same with that at rGO/MCH-S1/AuE, but the intensities of the two peaks decreased significantly, which suggested that some of the rGOs had been fallen off from the electrode surface. This also demonstrated that the probe DNA after assembly with rGO remained excellent hybridization efficiency.

In addition, from above electrochemical characterization experiment, it could be obtained that the EIS background signal of the DNA biosensor was greatly reduced by the transformation of attached GO to the reduced form. In order to investigate the effect of such a change on the performance of the biosensor, the signal variation ratio (SVR) of the DNA biosensor upon hybridization with target DNA sequence was determined according to the equation of $SVR=(R_{ct,after} - R_{ct,\ before})/R_{ct,before}$, and compared with the control electrodes of GO/MCH-S1/AuE and MCH-S1/AuE. The symbols of $R_{ct,after}$ and $R_{ct,before}$ in the equation represented the R_{ct} values of the biosensor before and after hybridization with target DNA.

Fig. 3 shows the Nyquist plots of GO/MCH-S1/AuE (A), rGO/MCH-S1/AuE (B), and MCH-S1/AuE (C) before (a) and after (b) hybridization with the same concentration (1.0×10^{-10} M) of target DNA (S2). The related R_{ct} values and the values of SVR were summarized in Fig. 3D. From the results, it could be observed that, for GO/MCH-S1/AuE, the R_{ct} value decreased slightly after hybridization with target DNA, from which a SVR value of -17% was obtained. Such a phenomenon could be ascribed to the fact that GO/MCH-S1/AuE itself had a very strong blocking effect to the electron transfer of $[Fe(CN)_6]^{3-/4-}$, which was induced by the cooperative electrostatic repulsion of probe DNA and GO; When the electrode was hybridized with target DNA, the double-helix DNA layer was formed at the electrode surface, making the adsorbed GO falling off from the electrode surface. However the increased repulsion force from the hybridized target DNA could not compensate the decrease of the repulsive force arising from the falling off of GO, therefore a decrease of R_{ct} value was achieved. For the traditional biosensor of MCH-S1/AuE, it was found that a large R_{ct} value of 35.0 kΩ was observed, and after hybridization with 1.0×10^{-10} M target DNA, the R_{ct} was increased to 68.2 kΩ. This change could be ascribed to the addition of the negative charge density from the hybridized target DNA strands. The SVR was determined to be 95%. It is interesting that when the rGO/MCH-S1/AuE was hybridized with target DNA, the R_{ct}

value of the biosensor was substantially increased from 7.4 kΩ to 64.2 kΩ, and the SVR value was obtained to be as large as 762%, demonstrating that the rGO-based biosensor has a very high signal-to-noise ratio.

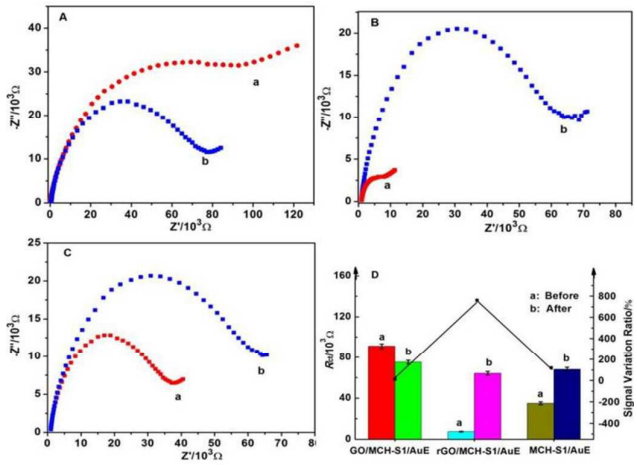

Fig. 3 Nyquist diagrams of 1.0 mM $[Fe(CN)_6]^{3-/4-}$ with 0.1 M KC1 at GO/MCH-S1/AuE (A), rGO/MCH-S1/AuE (B), MCH-S1/AuE(C) before (a) and after (b) hybridization with of 1.0×10^{-10} M S2. (D) Histogram of R_{ct} values of the different biosensors before (a) and after (b) hybridization with S2, and their corresponding signal variation ratio.

3.3 Optimization of the biosensor

In order to achieve the optimal performance of the biosensor, some experimental conditions such as accumulation time of GO, the reaction time of $NaBH_4$ with GO and hybridization time with target DNA were optimized by EIS technology. Fig. 4A shows the R_{ct} values versus incubation time (t_1) of MCH-S1/AuE in GO solution. From the figure, it was observed that with the increase of time, the R_{ct} values increased gradually, suggesting that more and more GO had been adsorbed to MCH-S1/AuE. When the self-assembly time reached 3 h, the R_{ct} values leveled off, indicating the adsorption saturation of GO on the electrode surface. Therefore, 3 h was used as the optimal time for the assembly of GO. The reaction time of $NaBH_4$ with GO to obtain rGO was also investigated by EIS. It was found that the R_{ct} values of the electrode decreased with the prolonging of the reaction time (t_2) of GO/S1/AuE in $NaBH_4$ solution (Fig. 4B), suggesting gradual reduction of GO by $NaBH_4$. When the time was upon 25 min, the R_{ct} value changed hardly, indicating the absolute reduction of GO on the electrode surface. Therefore, 25 min was chose as the optimal reaction time of $NaBH_4$ with GO. Figure 4C shows the relationship of R_{ct} values versus the reaction time of the biosensor with S2 (t_3). It was observed that with the increase of reaction time, the R_{ct} value increased gradually, indicating that more and more rGO had been fallen off from the electrode surface by the formed dsDNA. When the time reached to 45 min, the R_{ct} became a constant, which was an indication of the binding equilibrium between probe DNA and target DNA. Therefore, 45 min was selected as the optimal hybridization time of the biosensor with target DNA in this work.

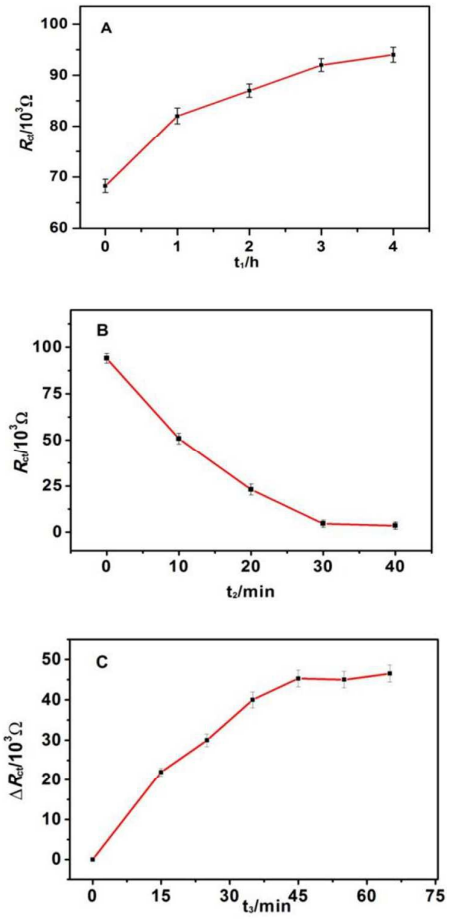

Fig. 4 (A) Effect of accumulation time (t_1) of GO on the R_{ct} values at the MCH-S1/AuE, and (B) relationship of R_{ct} values versus *in situ* reduction time (t_2). (C) Relationship of R_{ct} values versus incubation time (t_3) of rGO/MCH-S1/AuE in S2 solution. The standard deviation of three measurements was represented by the error bars. The concentration of S2 was 1.0×10^{-10} M.

3.4 Analytical performance of the DNA biosensor

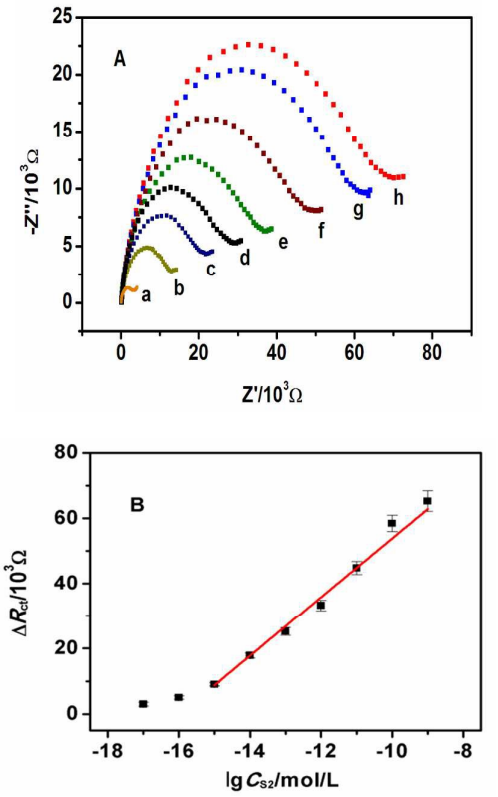

Fig. 5 (A) Nyquist diagrams of 1.0 mM $[Fe(CN)_6]^{3-/4-}$ with 0.1 M KC1 at rGO/MCH-S1/AuE before (a) and after its hybridization with 1.0×10^{-15} M (b), 1.0×10^{-14} M (c), 1.0×10^{-13} M (d), 1.0×10^{-12} M (e), 1.0×10^{-11} M (f), 1.0×10^{-10} M (g) and 1.0×10^{-9} M (h) S2. (B) The linear plot of ΔR_{ct} values versus the logarithm of S2 concentrations (lg C_{S2}). The standard deviation of three measurements was represented by the error bars.

Under the optimal conditions, the sensitivity of the DNA biosensor was evaluated by hybridization with the different concentrations of the target sequence (C_{S2}). Fig. 5A shows the EIS response of the developed biosensor upon hybridization with increasing concentrations of S2. As seen, when the concentration of S2 increased, the R_{ct} increased accordingly. This suggested that upon hybridization with increasing amount of target DNA, more and more highly conductive rGO were released from the electrode surface by the formed dsDNA. The difference value of R_{ct} (ΔR_{ct}) before and after hybridization showed a linear relationship with the logarithmic values of C_{S2} (lg C_{S2}) over a wide range from 1.0×10^{-15} M to 1.0×10^{-9} M. The linear equation was ΔR_{ct} (Ω) = 151.684+ 9621.5 lg(C_{S2}/M) with regression coefficient of R^2 = 0.9953 (Fig. 5B). The limit of detection is estimated to be as low as 2.9×10^{-16} M at signal-to-noise (S/N) of 3. The analytical performance of this proposed biosensor was also compared with some other electrochemical impedimetric DNA biosensors with $Fe(CN)_6]^{3-/4-}$ as indicator, and the results were listed in Table 1. It is apparent that the proposed DNA biosensor had the lower detection limit and the wider linear range for the target DNA than the other six biosensors, which could be ascribed to the low background response of the biosensor and the ingenious application of different binding force of rGO with ssDNA and dsDNA.

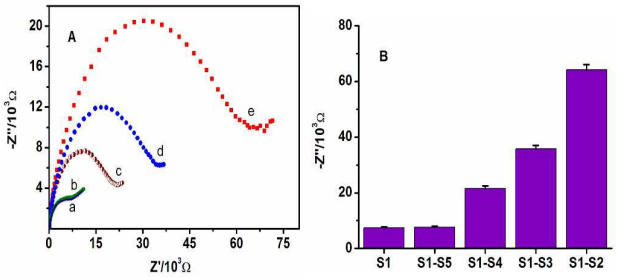

Fig. 6 Nyquist diagrams (A) and the corresponding histogram of R_{ct} values (B) on different hybridized electrodes. All the concentrations of hybridized sequences were 1.0×10^{-10} M. The standard deviation of three measurements was represented by the error bars.

The hybridization selectivity of the developed biosensor was further investigated by hybridization with various DNA sequences. Fig. 6 shows the obtained EIS of rGO/MCH-S1/AuE before (curve a) and after hybridization with fully complementary (S2, curve e), three-base mismatched (S4, curve c), one-base mismatched (S3, curve d) and noncomplementary (S5, curve b) sequences. It was clear that the value of R_{ct} in curve b was very close to that of curve a, suggesting that S5 had not been captured to the surface by S1 via hybridization reaction. While, after hybridization of the biosensor with the complementary sequences of S2, the obtained R_{ct} value extremely increased due to the formation of the intact duplex (curve e). Moreover, when one-base and three-base mismatched target sequences were hybridized, the obviously reduced R_{ct} values were observed (curve c and curve d, respectively), and meanwhile the R_{ct} values increased with the decrease of the base number of mismatch, further suggesting that the rGO-based biosensor had high selectivity to recognize the target sequences with different complementary degree.

3.5 Regeneration and stability of the DNA biosensor

The regeneration and stability are important properties of a DNA biosensor. In this work, the regeneration ability of the biosensor was investigated as the following procedures: the fabricated biosensor was immersed into a hybridization solution containing 1.0×10^{-11} M S2 for 45 min under 30 °C. After the electrochemical measurements, the DNA biosensor was incubated in 0.05 M NaCl at 80 °C

for 20 min and then cooled with ice-water. The results showed that by such a routine, the biosensor could be successively regenerated for at least five times without significant losing of its hybridization ability. In addition, the stability experiments showed that after a fabricated biosensor was stored at 4 °C in a dry environment for 4 weeks, the obtained R_{ct} value was very close to that before storage, suggesting that the biosensor had a good stability.

Table 1 Comparison of the analytical parameters with other impedimetric DNA biosensors

Biosensors	Linear ranges (M)	Detection limit (M)	Refs
DNA/Graphene/DEP	3.0×10^{-13}-3.0×10^{-10}	-	35
AuNPs/DNA/AuE	1.0×10^{-12}-5.0×10^{-7}	1.0×10^{-12}	36
PDI/Graphene/GCE	1.0×10^{-12}-1.0×10^{-6}	5.5×10^{-13}	37
DNA/GA-TRA-rGO/GCE	1.0×10^{-12}-1.0×10^{-7}	5.2×10^{-13}	38
DNA/GCE	1.0×10^{-12}-4.0×10^{-10}	1.5×10^{-13}	39
DNA/GTD/CS–MWNTs/GCE	1.0×10^{-13}-5.0×10^{-10}	8.5×10^{-14}	40
DNA/PXa-ERGNO/GCE	1.0×10^{-14}-1.0×10^{-8}	4.2×10^{-15}	41
rGO/MCH-DNA/AuE	1.0×10^{-15}-1.0×10^{-9}	2.9×10^{-16}	This work

Note: DEP: Dielectrophoresis; AuNPs: gold nanoparticles; PDI: perylenetetracarboxylic acid diimide; GA: glutaraldehyde; TRA–rGO: tryptamine-functionalized reduced graphene oxide; PXa-ERGNO: Poly(xanthurenic acid)-electrochemically reduced graphene oxide nanocomposite.

4 Conclusions

In this paper, the *in-situ* reduced GO (rGO) was used as a hybridization signal medium for the construction of a highly sensitive DNA biosensor. Through the unique π-π stacking with single-stranded probe DNA, the GO was adsorbed on the probe electrode surface. After reduction with $NaBH_4$, the GO on the electrode was changed to reduced form, which significantly decreased the background impendence response of the biosensor, due to its outstanding electronic conductivity. When the target DNA was hybridized, the DNA duplex structure was formed on the electrode surface, and the rGO were released from the electrode surface. Thus, the electronic transfer promotion effect by rGO was disappeared, and meanwhile the resistance was increased due to the formation of the ordered dsDNA. Through such a strategy, the sensing response (ΔR_{ct}) was greatly enlarged, resulting in an ultrahigh sensitivity for hybridization determination. This concept can also be utilized for construction of other oligonucleotides-based biosensors (such as aptasensors) for the detection of proteins, metal ions, cells and RNA.

Acknowledgements

The work is supported by the National Natural Science Foundation of China (No. 21275127), and Program for New Century Excellent Talents in Fujian Province University (No. JA12204).

Notes and references

1 R. Kong, Z. Song, H. Meng, X. Zhang, G. Shen, R. Yu, *Biosens. Bioelectron.* 2014, 54, 442.
2 L. Feng, Z. Zhang, J. Ren, X. Qu, *ACS Appl. Mater. Interfaces,* 2014, **6**, 3513.
3 Y. Hu, X. Xu, Q. Liu, L. Wang, Z. Lin, G. Chen, *Anal. Chem.,* 2014, **86**, 8785.
4 B. Zhu, M. Booth, P. Shepherd, A. Sheppard, J. Travas-Sejdi, *Biosens. Bioelectron.* 2015, **64**, 74.
5 R. Kong, Z. Song, H. Meng, X. Zhang, G. Shen, R. Yu, *Biosens. Bioelectron.* 2014, **54**, 442.
6 N. Aydemir, H. McArdle, S. Patel, W. Whitford, C. Evans, J. Travas-Sejdic, D. Williams, *Anal. Chem*. 2015, **87**, 5189.
7 Y. Du, B. Lim, B. Li, Y. Jiang, J. Sessler, A. Ellington, *Anal. Chem.* 2014, **86**, 8010.

8 E. Stejskalová, P. Horáková, J. Vacek, R. Bowater, M. Fojta, *Anal. Bioanal. Chem.* 2014, **406**, 4129.
9 W. Song, H. Li, H. Liang, W. Qiang, D. Xu, *Anal. Chem.* 2014, **86**, 2775.
10 A. Danhel, V. Raindlova, L. Havran, H. Pivonkova, M. Hocek, M. Fojt, *Electrochim. Acta* 2014, **126**, 122.
11 H. Wang, H. Ohnuki, H. Endo, M. Izumi, *Bioelectrochemistry* 2015, **101**, 1.
12 A. Erdem, G. Congur, *Int. J. Biol. Macromol.* 2013, **61**, 295.
13 A. Castela, B. Fonseca, R. Duarte, R. Neves, M. Montemor, *Electrochim. Acta* 2014, **124**, 52.
14 V. Hung, A. Veloso, A. Chow, H. Ganesh, K. Seo, E. Kendüzler, I. Brownb, K. Kerman, *Electrochim. Acta* 2015, **162**, 79.
15 H. Chen, Q. Mei, Y. Hou, X. Zhu, K. Koh, X. Li, G. Li, *Analyst* 2013, **138**, 5757.
16 J. Lin, Z. Wei, H. Zhang, M. Shao, *Biosens. Bioelectron.* 2013, **41**, 342.
17 P. Kongsuphol, H. Ng, J. Pursey, S. Arya, C. Wong, E. Stulz, M. Park, *Biosens. Bioelectron.* 2014, **61**, 274.
18 Z. Lin, X. Li, H. Kraatz, *Anal. Chem.* 2011, **83**, 6896.
19 Z. Lin, Y. Chen, X. Li, W. Fang, *Analyst* 2011, **136**, 2367.
20 Y. Zhu, Y. Cai, L. Xu, L. Zheng, L. Wang, B. Qi, C. Xu, *ACS Appl. Mater. Interfaces* 2015, **7**, 7492.
21 F. Gao, X. Cai, X. Wang, C. Gao, S. Liu, F. Gao, Q. Wang, Sensor. Actuat. B: Chem. 2013, 186, 380.
22 C. Wang, J. Kima, Y. Zhua, J. Yanga, G. Leec, S. Leed, J. Yue, T. Peif, G. Liub, C. Nuckollse, J. Honea, Q. Lin, *Biosens. Bioelectron.* 2015, **71**, 222.
23 B. Jana, A. Biswas, S. Mohapatra, A. Sahaa, S. Ghosh, *Chem. Commun.* 2014, **50**, 11595.
24 A. Bonanni, K. Chua, G. Zhao, Z. Sofer, M. Pumera, *ACS Nano* 2012, **6**, 8546.
25 J. Chen, X. Jiao, H. Luo, N. Li, *J. Mater. Chem. B* 2013, **1**, 861.
26 D. Wang, W. Hu, Y. Xiong, Y. Xua, M. Li, *Biosens. Bioelectron.* 2015, **63**, 185.
27 H. Zhang, S. Jia, M. Lv, J. Shi, X. Zuo, S. Su, L. Wang, W. Huang, C. Fan, Q. Huang, S *Anal. Chem*. 2014, **86**, 4047.
28 L. Wang, M. Xu, L. Han, M. Zhou, C. Z. Zhu, S. J. Dong, *Anal. Chem*. 2012, **84**, 7301.
29 A. Bourlinos, D. Gournis, D. Petridis, T. Szabó, A. Szeri, I. Dékány, *Langmuir* 2003, **19**, 6050.
30 [30] S. Park, J. An, J. Potts, A. Velamakanni, S. Murali, R. Ruoff, *Carbon* 2011, **49**, 3019.
31 P. He, J. Sun, S. Tian, S. Yang, S. Ding, G. Ding, X. Xie, M. Jiang, *Chem. Mater.* 2015, **27**, 218.
32 W. Hummers, R. Offeman, *J. Am. Chem. Soc.* 1958, **80**, 1339.
33 A. Michelle, MacDonald, A. Heather, Andreas, *Electrochim. Acta* 2014, **129**, 290.
34 Y. Guo, S. Guo, J. Ren, Y. Zhai, S. Dong, E. Wang, *ACS Nano* 2010, **4**, 4001.
35 A. Bonanni, M. Pumera, *ACS Nano* 2011, **5**, 2356.
36 Y. Yang, C. Li, L. Yin, M. Liu, Z. Wang, Y. Shu, G. Li, *ACS Appl. Mater. Interfaces* 2014, **6**, 7579.
37 Y. Hu, K. Wang, Q. Zhang, F. Li, T. Wu, L. Niu, *Biomaterials* 2012, **33**, 1097.
38 Z. Zhang, L. Luo, G. Chen, Y. Ding, D. Deng, C. Fan, *Biosens. Bioelectron.* 2014, **60**, 161.
39 M. Tabrizi, M. Shamsipur, *Biosens. Bioelectron.* 2015, **69**, 100.
40 Q. Wang, B. Zhang, X. Lin, W. Weng, Sensor. Actuat. B: Chem. 2011,**156**, 599.
41 T. Yang, Q. Li, L. Meng, X. Wang, W. Chen, K. Jiao, *ACS Appl. Mater. Interfaces* 2013, **5**, 3495.